

RESEARCH PAPER

X-ray and CO-Derived Column Densities in AGN: A Study of Obscuration Properties in CTAGN and Non-CTAGN

M. L. H. Musa,¹ Z. Z. Abidin,¹ A. Annuar,² and D. A. A. Lee¹

¹Department of Physics, Faculty of Science, Universiti Malaya, 50603 Kuala Lumpur, Federal Territory of Kuala Lumpur, Malaysia

²Department of Applied Physics, Faculty of Science and Technology, Universiti Kebangsaan Malaysia, 43600 UKM Bangi, Selangor, Malaysia

Author for correspondence: Zamri Zainal Abidin, Email: zzaa@um.edu.my.

(Received DD Mmm YYYY; revised DD Mmm YYYY; accepted DD Mmm YYYY; first published online DD Mmm YYYY)

Abstract

Obscuration in active galactic nuclei (AGN) provides valuable insights into the nature of the material surrounding the central engine. Compton-thick AGN (CTAGN), characterised by a column density of $N_{\text{H}} \geq 1.5 \times 10^{24} \text{ cm}^{-2}$, are heavily obscured by substantial amounts of dust and gas. While X-ray observations are primarily used to determine this column density, our understanding of obscuration properties in the sub-mm regime, particularly for CTAGN, remains limited. In this study, we analyse archival data from the Atacama Large Millimetre/sub-millimetre Array (ALMA) for both CTAGN and non-CTAGN sources, as identified by the 70-month catalogue of the all-sky hard X-ray *Swift*/Burst Alert Monitor survey and other X-ray surveys. Integrated intensity maps (moment 0) of CO(3–2) emission reveal a concentrated distribution of dense gas around the nucleus. Utilising a constant CO-to-H₂ conversion factor, $X_{\text{CO}} = 2.2 \times 10^{20} \text{ cm}^{-2} (\text{K km s}^{-1})^{-1}$, we find that the derived molecular hydrogen column densities, N_{H_2} , are generally lower than the total hydrogen column densities, N_{H} , obtained from X-ray observations. However, the N_{H_2} values derived in this work are slightly higher than those reported in previous studies due to the adoption of a higher CO-to-H₂ conversion factor. This discrepancy between N_{H} and N_{H_2} is consistent with prior findings that X-ray-derived column densities are typically higher, except in the case of non-CTAGN, where N_{H_2} can exceed N_{H} . Statistical analysis using Kendall and Spearman tests reveals a positive monotonic relationship between N_{H} and N_{H_2} , although the correlation is not statistically significant. This suggests a complex interplay of factors influencing these properties. The optically thick nature of CO in dense regions may contribute to the observed discrepancies. Our results highlight the importance of adopting an accurate CO-to-H₂ conversion factor to derive reliable column densities, which could serve as an alternative method for identifying CTAGN. Further investigations with more comprehensive data sets and refined methodologies are needed to better understand the relationship between sub-millimetre and X-ray properties in AGNs.

Keywords: active galactic nuclei—molecular gas

1. Introduction

Active galactic nuclei (AGN) are extremely bright compact regions at the centres 3% to 10% of galaxies (Gatica et al., 2023) and are more luminous ($L_{\text{bol}} \approx 10^{48} \text{ erg s}^{-1}$) than normal galaxies (Fabian, 1999). It is believed to play such a significant role in galaxy evolution (Kormendy & Richstone, 1995; Kormendy & Ho, 2013). Supermassive black holes (SMBHs) with masses, $M_{\text{SMBH}} \gtrsim 10^6 M_{\odot}$ are thought to power these regions. It is assumed that the intense radiation emitted by AGN is caused by material falling into the black hole, which heats up and emits energy as it is pulled in. AGN have been linked to the establishment of scaling relations between massive black holes (MBHs) and the properties of their host galaxies. They also regulate cooling flows in galaxy clusters, drive outflows across multiple scales, from the accretion disk to the circumgalactic medium, and contribute to the development of the red sequence in massive galaxies (Kormendy & Ho, 2013; Heckman & Best, 2014). The luminosities range from about 10^{40} erg/s to 10^{47} erg/s for distant quasars. One key aspect of AGN is obscuration, which refers to the amount of dust and gas that blocks our view of the nucleus. The obscuration can be characterised by the column density, N_{H} of the materials that lie along the line of sight.

Compton-thick AGN (hereafter, CTAGN) is a specific type of AGN where the nuclear emission is obscured by a significant amount of dust and gas. The intense emissions from AGNs, including X-rays, originate primarily from energetic particles surrounding the hot corona, which are accelerated and confined by magnetic fields at the accretion disk (Merloni & Fabian, 2001). These X-rays are often Compton-scattered to longer wavelengths (Antonucci, 1993), as they interact with dense clouds of dust and gas. In extreme cases, these X-ray emissions can be completely hidden from our observations because of heavy obscuration by dust and gas. Type 2 AGN, which include Seyfert 2 galaxies and type 2 quasars, are characterised by significant obscuration of the central engine. This obscuration is often attributed to their edge-on orientation relative to our line of sight, consistent with the AGN unification model (Antonucci, 1993). Understanding these sources can provide insights into the composition and dynamics of material surrounding the central engine, as well as how this material influences AGN obscuration.

Traditionally, identifying CTAGNs has been primarily accomplished through X-ray observations using instruments such as Chandra, XMM-Newton, and NuSTAR, where the column densities were derived from X-ray absorption. Since X-ray

observations are reliable against point source objects, for example, AGNs, we can easily distinguish them from other objects. However, sometimes other powerful objects, such as X-ray binaries, could also have the potential to contaminate these sources, despite also being often limited by the sensitivity of the instruments. For sources to be classified as AGN, the flux of X-ray point sources must be higher than $10^{42} \text{ erg s}^{-1}$, which is not the case for starburst galaxies ($< 10^{42} \text{ erg s}^{-1}$) (Jackson *et al.*, 2010). For a CTAGN, additional parameters need to be considered as well, which are the column densities, which it must be equal to or larger than the inverse of the Thomson cross-section $N_{\text{H}} \geq 1.5 \times 10^{24} \text{ cm}^{-2}$ (Comastri, 2004). The relationship between X-ray absorption and hydrogen column density is characterised by the fact that the hydrogen column densities, N_{H_2} inferred from X-ray absorption are typically 5-30 times higher than the neutral atomic hydrogen column densities, N_{HI} derived from $\lambda 21 \text{ cm}$ HI absorption toward radio-loud AGN (Liszt, 2021).

The relationship between X-ray-derived hydrogen column density, N_{H} and HI column density, N_{HI} is significant for understanding obscuration in AGN. Studies have shown that X-ray-derived column densities can often exceed total HI column densities along the same line of sight, indicating that additional sources of obscuration, such as molecular hydrogen or ionised gas, may be present (Liszt, 2021). This discrepancy emphasises the need for a comprehensive understanding of all gas components in AGN environments. Furthermore, a positive correlation between X-ray absorption and HI column density has been observed, suggesting that, as the X-ray column density increases, so does the HI column density, although this relationship may not always be statistically significant.

In recent years, there has been growing interest in finding alternative methods to measure the column density of AGN (e.g. Silver *et al.*, 2023; Silverman *et al.*, 2023; Torres-Albà *et al.*, 2023). One such approach is to use molecular hydrogen, H_2 which can provide a more accurate representation of the obscuration properties. It is important to note that there are different types of molecular gas being discussed. Warm H_2 , typically observed in the near-infrared and associated with temperatures ranging from 500 to 2000 K, differs significantly from cold molecular gas, which is often inferred from CO observations and generally exists at much lower temperatures (approximately 20 to 200 K).

Warm H_2 is typically found in regions of active star formation, where it can participate in processes that lead to the formation of stars. The higher temperatures of warm H_2 allow it to be excited by nearby stellar radiation, making it a key player in the dynamics of star-forming regions. In contrast, cold H_2 serves as the primary reservoir for star formation and is often found in dense molecular clouds, where conditions are favourable for gravitational collapse. CO does not always trace the same regions as warm or hot H_2 , making it essential to consider these differences when interpreting the physical conditions in AGN environments. While CO is a reliable tracer for cold, dense molecular gas, it primarily indicates regions that are cooler and may not capture the dynamics occurring in warmer gas phases. This distinction is crucial because CO emission can

sometimes arise from different physical conditions than those represented by warm H_2 .

Although measuring the molecular hydrogen, H_2 is quite challenging due to its weak emission, tracers such as CO can be used. CO is particularly useful for tracing the cold, dense molecular gas that forms stars and extreme regions such as AGN (e.g. Davies *et al.*, 2012; Esposito *et al.*, 2022, 2024). Due to its abundance and easy observability, CO also can provide crucial information about the physical properties of molecular clouds, such as their mass, density, temperature, and velocity structure. Hicks *et al.* (2009) discussed the role of molecular hydrogen in dense environments, particularly in obscuring regions in the central region of AGN. Their work highlights that the molecular hydrogen, H_2 can exceed the value ranges from 10^{22} up to 10^{24} cm^{-2} , with the inner radius of 100 pc in AGN.

In this work, we present a preliminary approach to explore the gap between total hydrogen column density, N_{HTotal} as derived from X-ray observation and molecular hydrogen column density, N_{H_2} , as described from sub-millimetre observation. We aim to assess whether molecular hydrogen column density N_{H_2} could serve as an alternative indicator of obscuration in AGN, and particularly help to search for CTAGN. Understanding this relationship could improve the method of identifying heavily obscured AGNs, as well as their nature of obscuration.

The paper is organised as follows: We describe the Atacama Large Millimetre/sub-millimetre Array (ALMA) observations of CTAGNs as well non-CTAGNs in section 2. In the same section, we discuss the steps in reducing the data obtained from the archive. In section 3, we present our main results, discussing the column density derived, and the correlation with X-ray column density. Finally, our conclusions are summarised in section 4. In this paper, we adopt a Λ CDM cosmology with parameters $H_0 = 70 \text{ km s}^{-1} \text{ Mpc}^{-1}$, $\Omega_m = 0.3$, and $\Omega_\Lambda = 0.7$.

2. Observations and Data Reduction

2.1 AGN Samples

In this study, we examine a sample of AGN characterised by a redshift, $z \leq 0.005$, while also distinguishing between CTAGN and non-CTAGN. This allows us to achieve high spatial resolution for imaging and spectroscopic data in the central regions of galaxies, where the dust that causes obscuration is present. At low redshift, spectral line measurements such as CO are less affected by redshift; thus it will improve the signal-to-noise ratio. Further considerations are their morphology (all are spirals, oriented roughly face-on towards the observer). The AGN sample was derived from the 70-month catalogue of the all-sky hard X-ray *Swift*/Burst Alert Monitor (*Swift*/BAT) survey (Baumgartner *et al.*, 2013), as reported by Ricci *et al.* (2017), which identified 838 AGNs, including 55 CTAGNs from Ricci *et al.* (2015). Subsequently, we searched for corresponding ALMA observations in the ALMA Science Archive, specifically targeting data on the CO(3-2) transition. Our investigation revealed a limited availability of data, with only five datasets corresponding to CTAGN and two datasets for non-CTAGN. To enhance comparability, we identified an additional three non-

CTAGN sources from the Chandra ACIS Survey for X-Ray AGN in Nearby Galaxies (CHANSNGCAT, She et al., 2017). As a result, we have 12 AGNs in total with 6 samples each for both CTAGN and non-CTAGN.

We utilised the NASA/IPAC Extragalactic Database (NED) to gather various properties of galaxies, including their celestial coordinates (RA and Dec), redshift values, morphology, and the types of AGN they contain. To ensure consistency, we crosschecked the AGN types obtained from NED/IPAC with data from The 70-Month *SWIFT*/BAT catalogue. Additionally, we sourced other properties, such as X-ray column density (N_{H}) and AGN location from past literature. Table 1 outlines the sample properties analysed in this study for easy reference

2.2 ALMA Observations

We utilised ALMA Band 7 (275 - 373 GHz) to observe the CO(3-2) transition at a rest frequency of 345.8 GHz in the central regions of our AGN sample. CO(3-2) is particularly effective for tracing dense gas in AGN environments due to its higher critical density ($n_{\text{crit}} = 3.6 \times 10^4 \text{ cm}^{-3}$; Carilli & Walter, 2013) compared to other CO transitions, such as CO(1-0) and CO(2-1). This high density sensitivity is important because Compton-thick AGNs (CTAGNs) are typically obscured by thick layers of dust and gas. Additionally, the CO(3-2) transition has an excitation temperature of around 33 K (Wilson et al., 2009), making it suitable for probing the relatively warm, dense molecular gas that characterises the obscuring regions in CTAGNs. Our analysis primarily relied on archival data sourced from the ALMA Science Archive. We systematically queried and acquired the pipeline data, thereby obtaining the cube file necessary for subsequent in-depth analysis. Table 2 lists all the ALMA observation properties obtained from the ALMA Science Archive.

2.2.1 Circinus Galaxy

Circinus Galaxy is a Seyfert 2 galaxy, hosting bright active galactic nuclei. Positioned 4 degrees below the Galactic plane, this galaxy is approximately 4.5 Mpc (Freeman et al., 1977), making it one of the closest major galaxies to our own. It is obscured by 100 pc scale dust lanes located at the galaxy plane (e.g. Wilson et al., 2000; Prieto et al., 2004; Mezcuca et al., 2016) and it became the ideal candidate for Compton-Thick galactic nuclei where the central emission suffers heavy obscuration and absorption along our line of sight. Greenhill et al. (2003b) observed H₂O maser emission where this traced a warped, edge-on accretion disk close to 0.1 pc from the nucleus. They provide initial evidence of dusty and high-density molecular material around the nucleus. They also suggested that this structure may be applied to other Seyfert 2 galaxies. A similar study by Hagiwara et al. (2021) investigated H₂O maser activity in the central regions of the AGN galaxies Circinus and NGC 4945 using ALMA at 321 GHz. They observed that the maser emissions in NGC 4945 show significant variability over 4-5 year timescales, with the nuclear continuum emission varying in correlation with the maser. However, this correlation is less

certain in the Circinus galaxy, where the relationship between maser and nuclear continuum emissions remains unclear.

The transition of CO(3-2) was observed in the central region of the Circinus galaxy by ALMA cycle 3 project (PID: 2015.1.01286.S, PI: Francesco Costagliola). This utilised ALMA band 7 (~350 GHz) receiver with the continuum sensitivity of 0.4602 mJy/beam. This galaxy was observed on 31st December 2015 and the pointing was centred at RA = 14^h13^m9.962^s, Dec = 65^d20^m20.937^s. The data were calibrated using the Common Astronomy Software Applications Package (CASA) version 4.5. This project aimed to study the dense interstellar medium of obscured AGN, at the centre of Circinus Galaxy.

2.2.2 NGC 1068

The galaxy NGC 1068 is one of the nearest Type 2 Seyfert galaxies to the Milky Way, with the Circinus galaxy being the closest known Seyfert. NGC 1068 is located in the constellation Cetus at a distance of approximately 14 Mpc (Bland-Hawthorn et al., 1997). Greenhill et al. (1996) produced the first VLBI synthesis images of the H₂O water maser emission originating from the galaxy's central engine. Among prior studies, Marinucci et al. (2015) analysed NuSTAR and XMM-Newton data and reported no spectral variations below 10 keV. Furthermore, numerous investigations have focused on the nuclear kinematics and molecular content of NGC 1068 (e.g., Jaffe et al., 2004; García-Burillo et al., 2016, 2017, 2019; Pfuhl et al., 2020), revealing distinct components: molecular gas emitting in the infrared, an X-ray-obscuring torus, and ionised gas (Wang et al., 2012). Using ALMA CO(3-2) observations, Imanishi et al. (2018) reported the detection of a rotating, elongated dense molecular emission associated with the torus in the nuclear region of NGC 1068. Their findings suggest that the molecular emission rotates predominantly in the east-west direction and exhibits significant inhomogeneity, with the western region of the AGN being notably more turbulent than the eastern region.

For ALMA CO(3-2) observation, the data was taken from archival data (PID: 2016.1.00232.S, PI: Santiago Garcia-Burillo). This project aims at the circumnuclear region of NGC 1068, covering the region from ~100 pc radius down to 7~ 10 pc of torus diameter. The continuum sensitivity of this target was 0.0306 mJy/beam. This observation was conducted on 8th September 2017 with the telescope pointing at RA = 2^h42^m40.711^s, Dec = -00^d00^m47.840^s. The data were calibrated using CASA version 4.7.2.

2.2.3 NGC 4945

NGC 4945 is a nearby edge-on Seyfert II galaxy with a visible obscuring dust lane in the central region. It is one of the brightest radio-quiet Seyfert in 100 keV surveys (Done et al., 1996) and displays both Seyfert (Schurch et al., 2002) and starburst (Bendo et al., 2016; Emig et al., 2020). A recent study by Bolatto et al. (2021) using ALMA has detected molecular outflows of CO (3-2), HCO⁺ and HCN in the central region of NGC 4945. The molecular outflow plumes align with the edges of the ionised gas outflow, tracing a receding cone that

Table 1. Properties of the AGN sample used in this work, were obtained from the NASA/IPAC Extragalactic Database (NED).

Source Name	RA _{J2000} (h:m:s)	Dec _{J2000} (d:m:s)	Morphology	AGN Type	z
Compton-Thick AGN					
Circinus Galaxy	14:13:09.950	-65:20:21.20	SA(s)b:	Sy2	0.00140
NGC 1068	02:42:40.711	-00:00:47.81	(R)SA(rs)b	Sy2	0.00380
NGC 4945	13:05:27.477	-49:28:05.57	SB(s)cd: edge-on	Sy2	0.00190
NGC 5643	14:32:40.743	-44:10:27.86	SAB(rs)c	Sy2	0.00399
NGC 6240	16:52:58.871	+02:24:03.33	I0: pec	Sy1.9	0.00245
NGC 7582	23:18:23.500	-42:22:14.00	(R')SB(s)ab	Sy2	0.00525
Non-Compton-Thick AGN					
NGC 613	01:34:18.170	-29:25:06.10	SB(rs)bc	Sy/LINER	0.00500
NGC 1097	02:46:19.05	-30:16:29.6	SB(s)b	LINER b	0.00424
NGC 1566	04:20:00.42	-54:56:16.1	SAB(s)bc	Sy1.5	0.00500
NGC 1808	05:07:42.34	-37:30:47.0	(R)SAB(s)a	-	0.00334
NGC 6300	17:16:59.47	-62:49:14.0	SB(rs)b	Sy2	0.00370
NGC 7314	22:35:46.19	-26:03:01.68	SAB(rs)bc	Sy1.9	0.00480

is obscured behind the galaxy disk and undetectable in optical or soft X-ray emission. Another study using ALMA Band 3 observation was carried out by Henkel *et al.* (2018) to study the structure, dynamics, and composition of NGC 4945. Most observed molecular lines show absorption near the nuclear millimetre-wave continuum source, especially between -60 and $+90$ km s⁻¹ from the systemic velocity of 571 km s⁻¹. Only the CH₃C₂H J=5→4 transition is unaffected, likely due to its lower critical density, with line emission absorbed slightly southwest of the continuum peak.

This galaxy is observed by ALMA (PID: 2018.1.01236.S, PI: Adam Leroy) on December 8, 2018, using a telescope pointing centred on a right ascension RA = 13^h05^m27.476^s and a declination Dec = -49^d28^m05.100^s. Data acquisition achieved a continuum sensitivity of 0.0341 mJy/beam. The calibration was performed using CASA version 5.4.0-68. The project aims to observe the nuclear starburst region of NGC 4945 to confirm and study ~20 candidate super star clusters identified in previous ALMA imaging. They will measure the clusters' dynamical mass, gas mass, dust opacity, and stellar content by utilising ALMA Band 3 and 7.

2.2.4 NGC 5643

NGC 5643, located in the constellation Lupus, is an active galaxy that has been extensively studied, particularly in optical and X-ray wavelengths. For instance, Annuar *et al.* (2015) utilised NuSTAR observations, in combination with previous X-ray data, to directly measure the obscuring column and confirm the classification of the galaxy's X-ray source. García-Bernete *et al.* (2021) employed ALMA CO(2-1) observations to study the cold molecular gas and MUSE IFU optical emission lines to investigate the ionised gas, aiming to explore the multiphase feedback processes at the central AGN of NGC 5643. Similarly, Alonso-Herrero *et al.* (2018) analysed ALMA Band 6 ¹²CO(2-1) line and rest-frame 232 GHz continuum observations, revealing that the ¹²CO(2-1) kinematics can be

modelled as a rotating disk, which appears tilted relative to the galaxy's large-scale disk. Additionally, they identified strong non-circular motions in the central 0.2–0.3 arcseconds of the galaxy, with velocities reaching up to 110 km/s.

ALMA observation of NGC 5643 was performed on April 19th, 2018 (PID: 2017.1.00082.S, PI: Santiago Garcia-Burillo), targeting the molecular tori to study its characteristics in Seyfert 2 AGN. This project was proposed to map the circumnuclear region using CO(3-2) and HCO⁺(4-3) of 10 Seyfert galaxies, including NGC 7582, which is also one of the samples in this paper. The telescope pointing was at RA = 14^h32^m40.778^s and Dec = -44^d10^m28.600^s with the continuum sensitivity of 0.0496 mJy/beam. The data calibration was done using CASA version 5.1.1-5.

2.2.5 NGC 6240

NGC 6240 is an Ultraluminous Infrared Galaxy (ULIRG) that hosts a double-nucleus AGN, first identified by Komossa *et al.* (2003) using X-ray spectroscopy with the *Chandra* X-ray Observatory. High-resolution imaging revealed the presence of a double AGN, confirmed by the detection of two prominent neutral Fe K α lines. However, recent research has uncovered a third nucleus, indicating a triple AGN system in the final stages of merging (Kollatschny *et al.*, 2020). This finding, confirmed through MUSE observations, resolved the previously identified double nucleus region. Additionally, Treister *et al.* (2020) reported a bulk of molecular gas within approximately 1" of the region between the two nuclei, as traced by ALMA Band 6 observations of ¹²CO(2-1) emission.

NGC 6240 was observed on May 4th, 2015 on the Cycle 2 project (PID: 2013.1.00813.S, PI: Naseem Rangwala) with the telescope pointing centred at RA = 16^h52^m58.861^s and Dec = +02^d24^m03.550^s, achieving angular resolution of 0.176 arcseconds and continuum sensitivity of 0.1258 mJy/beam. The reduction was done using CASA version 4.3.1 and calibrated using the pipeline. The observations were conducted under the

Table 2. ALMA Observation Properties

Source Name	Project ID	Observation Date	Angular Resolution (arcsec)	Velocity Resolution (km/s)	FOV (arcsec)	Continuum Sensitivity (mJy/beam)	Line Sensitivity (mJy/beam)	Vlsr Used (km/s)
Compton-Thick AGN								
Circinus Galaxy	2015.1.01286.S	2015-12-31	0.910	6.587	61.511	0.4602	11.282	433.79
NGC 1068	2016.1.00232.S	2017-09-08	0.033	3.302	16.593	0.0306	0.686	1137.78
NGC 4945	2018.1.01236.S	2018-12-08	0.317	1.635	16.659	0.0341	0.923	537.73
NGC 5643	2017.1.00082.S	2018-04-19	0.462	3.303	16.690	0.0496	1.317	1191.43
NGC6240	2013.1.00813.S	2015-05-04	0.176	6.649	16.907	0.1258	3.098	7118.11
NGC 7582	2017.1.00082.S	2018-08-30	0.329	3.307	16.674	0.0687	1.587	1569.91
Non-Compton-Thick AGN								
NGC 613	2016.1.00296.S	2016-11-23	0.294	0.827	16.705	0.0549	1.385	1477.01
NGC 1097	2015.1.00126.S	2016-09-14	0.099	3.301	16.694	0.0304	0.748	1259.22
NGC 1566	2016.1.00296.S	2016-11-24	0.315	0.827	16.706	0.0608	1.532	1502.42
NGC 1808	2015.1.00404.S	2016-08-12	0.150	3.298	16.685	0.0632	1.538	998.80
NGC 6300	2017.1.00082.S	2018-08-22	0.544	3.302	16.684	0.0576	1.393	1100.19
NGC 7314	2017.1.00082.S	2018-08-30	0.330	3.306	16.703	0.0682	1.616	1423.51

project to map the warm gas morphologies of the galaxy that undergoing a merging state of luminous infrared galaxies.

2.2.6 NGC 7582

NGC 7582 is a nearby Seyfert 2 galaxy exhibiting a Seyfert/starburst composite nature (Wold et al., 2006). Its nucleus is heavily obscured by dust, likely associated with a torus structure (Regan & Mulchaey, 1999). X-ray studies, including observations by NuSTAR, indicate that NGC 7582 contains a hidden nucleus obscured by a torus covering approximately 80%–90% of the line of sight (Rivers et al., 2015). Additionally, Braito et al. (2017) provide a high-resolution map of the nucleus from *Chandra* observations, showing that the soft X-ray emission originates from a hybrid gas ionised both by intense circumnuclear star formation and the central AGN. Furthermore, NGC 7582 has been extensively studied for its dusty molecular gas content using ALMA, as explored in recent works by Almeida et al. (2022) and García-Burillo et al. (2021).

Observations towards NGC 7582 were carried out on August 30th, 2018 (PID: 2013.1.00813.S, PI:Santiago Garcia-Burillo). The telescope was pointed at RA = $23^{\text{h}}18^{\text{m}}23.621^{\text{s}}$ and Dec = $-42^{\text{d}}22^{\text{m}}14.060^{\text{s}}$ with the continuum sensitivity reached 0.0687 mJy/beam. Data processing and analysis were conducted using CASA software, version 5.1.1-5. The project aims to investigate the presence and characteristics of molecular tori in Seyfert galaxies, which are thought to obscure the broad-line region around supermassive black holes in Type-2 AGN.

2.2.7 NGC 613

One of the earliest observations on this galaxy was carried out by Blackman (1981) using 17 long-slit spectrograms. Coincidentally, he also observed the galaxies NGC 1097 and NGC 1365. Observations in radio wavelengths on this galaxy have also been conducted using the Very Large Array (VLA) such as

in Hummel et al. (1987). More recent work using the ALMA is exemplified by Miyamoto et al. (2017). In it, the authors studied NGC 613 using the ALMA Bands 3 and 7, which covered the frequency range of 90 – 350 GHz. The molecules observed included CO(3-2), HCN(1-0), and others in the circumnuclear disk and ring in the nucleus of the galaxy. A work by Audibert et al. (2019) suggested a filamentary structure that connects the nuclear to the spiral arms, highlighting a two-arm trailing nuclear spiral, a circumnuclear star-forming ring, and evidence of AGN-driven molecular outflows. Their findings also indicate efficient angular momentum loss, facilitating inflow of molecular gas toward the central black hole.

NGC 613 observations were conducted on November 23rd, 2016, a cycle 3 ALMA observation (PID: 2016.1.00296.S, PI: Françoise Combes). This observation was centred on RA = $01^{\text{h}}34^{\text{m}}18.235^{\text{s}}$ and Dec = $-29^{\text{d}}25^{\text{m}}06.560^{\text{s}}$ with the angular resolution of 0.290 arcsec. The reduction and calibration were done using CASA version 4.7.0-1. Under the same project, NGC 613 and NGC 1566 were observed to explore the various conditions in the AGN and star formation environment.

2.2.8 NGC 1097

We also examined the barred spiral galaxy NGC 1097, located in the constellation Fornax. This galaxy hosts a LINER/Seyfert 1 nucleus and was initially classified as a LINER (Low-Ionisation Nuclear Emission Line Region) by Heckman (1980). A double-peaked Balmer line feature was later discovered by Storchi-Bergmann et al. (1993). Due to the low bolometric luminosity ($L_{\text{Bol}} = 8.6 \times 10^{41} \text{ergs}^{-1}$, Nemmen et al. (2006)), this galaxy also classified as low-luminosity AGN (LLAGN, bolometric luminosity, $L_{\text{Bol}} \lesssim 10^{42} \text{ergs}^{-1}$, Ho (2008)). Prieto et al. (2019) studied this galaxy across infrared to ultraviolet wavelengths and reported that the observed star formation rate is inconsistent with the available gas reservoir. Using ALMA CO(3-2) observations, Izumi et al. (2017) mapped the cold gas

distribution and suggested that the torus in NGC 1097 is thinner compared to that in NGC 1068 (García-Burillo *et al.*, 2016). Additionally, dynamical modelling of the CO(3–2) velocity field indicates that the cold molecular gas is concentrated in a thinner layer than the hot gas, which is traced by the $2.12 \mu\text{m}$ H₂ emission, within and around the torus.

For NGC 1097, the ALMA observation was carried out on September 14, 2016 (PID: 2015.1.00126.S, PI: Takuma Izumi) on cycle 3 project, reaching angular resolution of around 0.099 arcseconds. The velocity resolution was 3.301 km/s, and the field of view was approximately 16.694 arcseconds. The continuum sensitivity was 0.0304 mJy/beam, and the line sensitivity was 0.748 mJy/beam. The Vlsr used for this observation was 1259.22 km/s. The observation was centred on RA = $02^{\text{h}}46^{\text{m}}19.059^{\text{s}}$ and Dec = $-30^{\text{d}}16^{\text{m}}29.680^{\text{s}}$

2.2.9 NGC 1566

NGC 1566 is a nearby barred spiral galaxy exhibiting Seyfert characteristics (Shobbrook, 1966) and later classified as a Seyfert 1. It is one of the brightest galaxies in the Dorado group, with a centrally symmetric structure as observed in spectroscopic and kinematic studies (Agüero *et al.*, 2004). Recent study has revealed a “changing-look” feature in the AGN of NGC 1566, marked by dramatic outbursts across multiple wavelengths and shifts in optical and X-ray properties. Although it is classified as a changing-look AGN, some studies suggest it harbours a low-luminosity AGN (LLAGN) (Koribalski *et al.*, 2004). Smajić *et al.* (2015) investigated the LLAGN the nuclear disk of NGC 1566 using ALMA and SINFONI, revealing significant molecular hydrogen within the disk ($r = 3''$) and a spiral structure extending through disk. Also, the work by Combes *et al.* (2014) used ALMA CO(3–2) observations to probe the inner structure of NGC 1566, revealing a molecular trailing spiral spanning 50 to 300 pc, located at the inner Lindblad resonance (ILR) ring. This spiral efficiently channels gas toward the nucleus, suggesting AGN fueling through spiral-driven inflows. Their analysis of HCN(4–3) and HCO⁺(4–3) emission indicates that star formation dominates over AGN heating.

The ALMA observation of NGC 1566 was conducted on November 24, 2016 (PID:2016.1.00296.S, PI: Françoise Combes), a cycle 4 project, and achieved an angular resolution of approximately 0.315 arcseconds. The velocity resolution of the observation was around 0.827 km/s, and the field of view was roughly 16.706 arcseconds. The continuum sensitivity of the observation was about 0.0608 mJy/beam, while the line sensitivity was approximately 1.532 mJy/beam. The Vlsr (local standard of rest velocity) used for this observation was 1502.42 km/s.

2.2.10 NGC 1808

NGC 1808 is a nearby Seyfert 2 galaxy located at a distance of 9.5 Mpc (Tully *et al.*, 2016). It is identified as a barred galaxy, as revealed by the distribution of neutral hydrogen (Phillips, 1993), and is also classified as a starburst galaxy. Notably, it exhibits peculiar “hot spots” in its central 500 pc star-

forming region, which contain supernova remnants and young star clusters (Sérsic & Pastoriza, 1965; Galliano & Alloin, 2008). NGC 1808 has been extensively studied for its gas kinematics and structural features using ALMA observations (e.g., Salak *et al.*, 2016; Audibert *et al.*, 2021; Chen *et al.*, 2023). These studies have confirmed the presence of a compact circumnuclear disk (CND) within $r < 200$ pc and a distinct nuclear spiral structure traced by dense gas tracers, including the HCN(4–3), HCO⁺(4–3), and CS(7–6) lines.

The observation for NGC 1808 was carried out on August 12, 2016 (PID: 2015.1.00404.S, PI: Françoise Combes), which on cycle 3 as Additional Representative Images for Legacy (ARI-L) products. The angular resolution achieved was 0.150 arcseconds with the velocity resolution of 3.298 km/s. The telescope pointing was centred at RA = $05^{\text{h}}07^{\text{m}}42.343^{\text{s}}$ and Dec = $-37^{\text{d}}30^{\text{m}}46.980^{\text{s}}$. The data reduction was done using CASA version 4.5.3 while for ARI-L processing, the CASA version used was 5.6.1-8. The observation of NGC 1808 was part of the project that characterised and quantified the molecular outflows of 20 AGNs on ~ 100 pc scales.

2.2.11 NGC 6300

NGC 6300 is classified as a Seyfert 2 galaxy (Phillips *et al.*, 1983) and exhibits SBb-type morphology. Located in the southern hemisphere, this ring-barred galaxy features a clumpy, non-uniform torus revealed through X-ray observations from instruments such as Suzaku, the Chandra X-ray Observatory, and the Nuclear Spectroscopic Telescope Array (NuSTAR) (Jana *et al.*, 2020). These observations suggest that the nuclear region is Compton-thin, with properties such as line-of-sight column density, intrinsic luminosity, and the Fe K α emitting region showing variability and potential evolution over time. A previous study by Awaki *et al.* (2005) detected rapid time variability through timing analysis using XMM-Newton data. This variability indicates that NGC 6300 hosts a Seyfert 1 nucleus obscured by dense material surrounding it. These findings further support the unified AGN model, where classification is primarily determined by the degree of obscuration.

The ALMA observation of NGC 6300 was carried out on 22 August 2018 (PID: 2017.1.00082.S, PI: Santiago Garcia-Burillo), achieving an angular resolution of 0.544 arcseconds. The velocity resolution was 3.302 km/s, and the field of view was around 16.684 arcseconds. The continuum sensitivity was 0.0576 mJy/beam, and the line sensitivity was 1.393 mJy/beam. The Vlsr used for this observation was 1100.19 km/s. The observation was centred at RA = $17^{\text{h}}16^{\text{m}}59.473^{\text{s}}$ and Dec = $-62^{\text{d}}49^{\text{m}}13.980^{\text{s}}$. The CASA version used for calibration was CASA version 5.1.1.

2.2.12 NGC 7314

NGC 7314, located in the constellation Piscis Austrinus, hosts a nucleus with classifications ranging from Seyfert 1.9 to Seyfert 2. While some studies classify it as Seyfert 1 (Stauffer, 1982; Morris & Ward, 1985; Schulz *et al.*, 1994), others identify it as Seyfert 2 (Nagao *et al.*, 2000; Trippe *et al.*, 2010), reflecting the complexity and variability of its nucleus, as demonstrated

by the variability of X-rays (e.g. Yaqoob et al., 1996; Turner et al., 1997). A recent study of X-ray variability using XMM-Newton observations explored this variability in depth through power spectral density (PSD) analysis, a method used to examine the frequency-dependent behavior of these variations (Emmanoulopoulos et al., 2016). The findings suggest that the variability follows a model with a bending frequency, indicating distinct behaviors above and below this frequency. Furthermore, da Silva et al. (2023) conducted a detailed multiwavelength analysis of the nuclear region of NGC 7314, investigating properties such as emission-line spectra, the morphology of the line-emitting regions, and spectral variability.

ALMA observation of NGC 7314 was conducted on August 30, 2018 (PID:2017.1.00082.S ,PI: Santiago Garcia-Burillo), with an angular resolution of approximately 0.330 arcseconds. The telescope pointing was centred at RA = 22^h35^m46.230^s, Dec = -26^d03^m00.900^s. The velocity resolution was 3.306 km/s, and the field of view was around 16.703 arcseconds. The continuum sensitivity was 0.0682 mJy/beam, and the line sensitivity was 1.616 mJy/beam. The Vlsr used for this observation was 1423.51 km/s. The data calibration was done using CASA version 5.1.1-5 and Pipeline-CASA51-P2-B r40896. Under the same project with NGC 5643, NGC 7582, and NGC 6300, their main goal is to map the CO(3-2) and HCO⁺ lines within the circumnuclear region of 10 nearby Seyfert galaxies, utilising data from ultra-hard X-ray selected AGN in the Galaxy Activity, Torus, and Outflow Survey (GATOS; García-Burillo et al., 2021; García-Burillo et al., 2024) sample.

2.3 Data Reduction

We utilised pipeline data retrieved from the ALMA Science Archive, focusing on the primary beam-corrected CO(3-2) spectral line data. Once the Flexible Image Transport System (FITS) files were obtained, we applied a 3 σ clipping to the data cubes to eliminate unwanted background sources, distinguishing them from the central sources of interest. This process also enhanced the signal-to-noise ratio. The final images were much clearer, with reduced background emission. All analyses were conducted using the Astropy SpectralCube package.

Since the ALMA observations for each sample were conducted during different cycles and used different versions of the CASA software, we opted not to re-calibrate the data. Instead, we used the calibrated pipeline data available in the archive, specifically searching for CO(3-2) emission line cube data. The line detection was confirmed using the ALMA Data-Mining Toolkit (ADMIT), accessible through the cube web preview on the ALMA Science Archive. All calibrated pipeline data were corrected for the primary beam.

3. Results and Discussions

3.1 Integrated Intensity Maps

To analyse the distribution of CO(3-2) around the nucleus, we generated the integrated intensity map (moment 0 map) for all samples using the SpectralCube task `cube.moment(order=0)`. We used the noise-reduced data cubed to generate the moment 0, producing cleaner and lower

noise results. To study the gas distribution around the nucleus, we focused on the nuclear region, covering an area from 0.2 to 6 arcseconds. We then collapsed over the entire range of velocity channels in each data cube to create moment 0 maps over this region. The parameters used are provided in Table 3.

Figure 1(i) and 1(ii) present the integrated intensity maps for the CTAGN and non-CTAGN sources. The size of each galaxy region varies according to the extent of the nuclear region; thus, we standardised the region size to a square pixel grid. To ensure a clear and consistent comparison of the CO(3-2) emission distribution and concentration, we standardised the intensity scale values to $I_{\text{CO}_{\min}} = 0 \text{ K km s}^{-1}$ and $I_{\text{CO}_{\max}} = 10^4 \text{ K km s}^{-1}$. AGN positions, primarily determined through radio observations and referenced from previous literature, are marked by cyan stars, while the emission peaks in the moment 0 maps are indicated by cyan crosses. The yellow contour marks the CTAGN region, where we derived the corresponding threshold for the I_{CO} from the column density to identify the CTAGN regions. The N_{H_2} values were calculated using a conversion factor, which is discussed in detail in Section 3.2.

A comparison between the AGN positions from the literature and the CO(3-2) integrated intensity peaks reveals notable spatial offsets. This study aims to explore the spatial relationship between the CO(3-2) intensity peak, which we define as the brightest pixel in the integrated intensity map, and the AGN positions documented in the literature. It is worth noting that the CO(3-2) peak does not necessarily align with the AGN position, as several ALMA studies have shown that AGN positions are often traced by the 300 GHz continuum peak, while the CO(3-2) emission can be influenced by other processes such as star formation, circumnuclear rings, or nuclear spirals (e.g. Izumi et al., 2018; Audibert et al., 2021; Tristram et al., 2022; Combes, 2023). Table 4 lists all the AGN positions derived from the literature alongside the separation offsets between these positions and the CO(3-2) integrated intensity peaks.

CO(3-2) is a well-known dense gas tracer commonly used to map the distribution of molecular gas in obscured environments, such as those surrounding AGN (e.g., Tsai et al., 2012; Miyamoto et al., 2017; Alonso-Herrero et al., 2018; Kawamuro et al., 2019; Lamperti et al., 2020; Jones et al., 2023). It provides valuable insights into AGN-related processes, including radiation and outflows, which can significantly affect the gas reservoir of the host galaxy (Circoستا et al., 2021). Additionally, CO(3-2) is particularly useful for tracing cold dense molecular gas, which forms key components of structures such as the torus and circumnuclear disk (CND).

The CO(3-2) moment 0 maps generated for the observed galaxies highlight distinct morphological differences between CTAGN and non-CTAGN sources. For CTAGN sources, such as NGC 1068, NGC 4945, and NGC 6240, the CO(3-2) emission is strongly concentrated in the nuclear regions, with peaks located near the AGN positions. This indicates a significant accumulation of cold molecular gas around the AGN, likely associated with circumnuclear material, such as a torus. Notably, NGC 1068 also exhibits extended structures, including faint, elongated features that could be linked to AGN-driven

Table 3. Region sizes and velocity widths used in the observed sample.

Source Name	Region Size		Velocity Width
	(deg)	(arcsec)	(km/s)
Compton-Thick			
Circinus Galaxy	0.001667×0.001667	6.000×6.000	235.000 - 1283.390
NGC 1068	0.000061×0.000061	0.220×0.220	-400.000 - 280.000
NGC 4945	0.001497×0.001497	5.390×5.390	-257.184 - 1366.301
NGC 5643	0.000989×0.000989	3.560×3.560	398.826 - 2014.197
NGC 6240	0.001044×0.001044	3.760×3.760	-500.000 - 480.000
NGC 7582	0.001675×0.001675	6.030×6.030	757.917 - 2373.377
Non Compton-Thick			
NGC 613	0.000542×0.000542	1.950×1.950	1195.216 - 1770.591
NGC 1097	0.000550×0.000550	1.980×1.980	455.395 - 2069.845
NGC 1566	0.001389×0.001389	5.000×5.000	704.350 - 2314.350
NGC 1808	0.000467×0.000467	1.680×1.680	201.742 - 1820.268
NGC 6300	0.000758×0.000758	2.730×2.730	304.768 - 1920.293
NGC 7314	0.000775×0.000775	2.790×2.790	621.571 - 2237.008

outflows. In contrast, other CTAGN sources, such as the Circinus galaxy, NGC 5643, and NGC 7582, show weaker emission concentrated near the AGN positions but also display extended components. These features may reflect the presence of nuclear spiral arms or star-forming regions, which could contribute to the observed gas outflows. For non-CTAGN sources, the CO(3–2) emission appears more extended and less concentrated in the nuclear regions compared to CTAGN sources. A relatively low concentration of CO(3–2) is clearly observed in NGC 1566 and NGC 7314, further supporting the idea that the cold molecular gas is distributed across larger areas rather than being confined to the centre. In cases such as NGC 1097 and NGC 1566, the emission exhibits irregular distributions, with peaks offset from the AGN positions, reflecting the dynamic nature of the gas in these systems.

Figure 1(i) demonstrates stronger CO(3–2) concentration around the nuclear regions of CTAGN, while Figure 1(ii) illustrates the more dispersed emission characteristic of non-CTAGN. These differences align with the understanding that CTAGN are surrounded by dense, thick obscuring material, leading to compact emission in the nuclear region. Although extended structures are present in both CTAGN and non-CTAGN, they appear to be more pronounced in non-CTAGN. This may be due to less dense surrounding material in non-CTAGN, allowing for a broader distribution of the cold molecular gas.

In previous related studies, the Galaxy Activity, Torus, and Outflow Survey (GATOS, García-Burillo *et al.*, 2021; García-Burillo *et al.*, 2024) investigated the dusty molecular tori properties of nearby Seyfert galaxies. The first results of this project, presented by García-Burillo *et al.* (2021), revealed spatially resolved CO(3-2) and HCO⁺(4-3) emissions in disks surrounding AGN. While CO(3-2) is frequently detected in AGN, its emission typically does not peak at the centre. Instead, it is more commonly observed in regions surrounding the AGN, often associated with structures such as rings or the edges of cavities formed by outflows. This could explain the notable

offset of CO(3–2) peak integrated intensity, I_{CO} from the AGN position obtained from the previous literature, shown in Figure 1. Furthermore, the study quantified the central concentration of molecular hydrogen (H₂) on various spatial scales, linking H₂ surface density with AGN luminosities and Eddington ratios. A deficit of molecular gas was identified in the nuclear regions, particularly in AGN with higher luminosities and Eddington ratios. This finding suggests that AGN feedback, which is stronger in more luminous AGN, plays a crucial role in redistributing or depleting molecular gas from the nuclear regions.

3.2 Molecular Hydrogen Column Density

The moment 0 peak values were determined, and their corresponding positions are provided in Table 4. The moment 0 map of CO(3–2) highlights a concentrated emission near the nucleus, suggesting the presence of a highly obscuring medium within the size of approximately 10 to 100 pc around the nucleus. Using the moment 0 CO(3-2) peak integrated intensity value, we derived molecular hydrogen column density, N_{H_2} using CO-to-H₂ conversion factor. We converted the intensity value from Jy/beam to K using the standard brightness temperature relation on the original cube file before proceeding with moment 0 maps. Equation (1) shows the method of deriving the molecular hydrogen column density, N_{H_2} obtained from Rahmani *et al.* (2016).

$$N_{\text{H}_2} (\text{cm}^{-2}) = X_{\text{CO}} \times I_{\text{CO}} \quad (1)$$

where N_{H_2} is the molecular hydrogen column density, X_{CO} is the CO-to-H₂ conversion factor, and I_{CO} is the CO integrated intensity in K kms⁻¹. We adopted a constant Milky Way conversion factor, $X_{\text{CO}} = 2.2 \times 10^{20} \text{cm}^{-2} (\text{K km s}^{-1})^{-1}$ from Solomon *et al.* (1983) which corresponds to $\alpha_{\text{CO}} = 3.5 M_{\odot} \text{pc}^{-2} (\text{K km s}^{-1})^{-1}$.

The derived molecular hydrogen column density, N_{H_2}

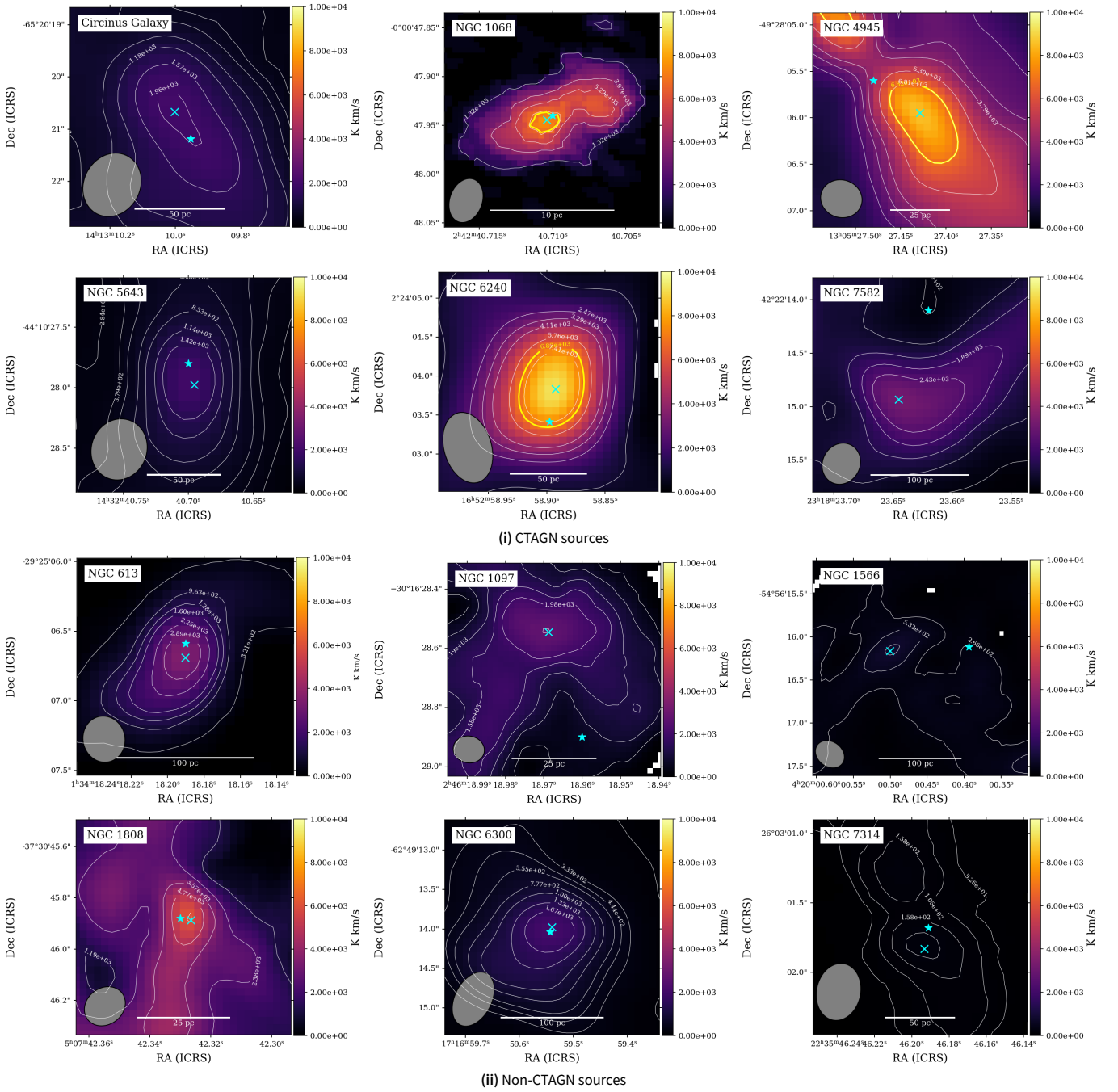


Figure 1. CO(3-2) Integrated Intensity (Moment 0) of CTAGN and non-CTAGN sources. The cyan cross marks the integrated CO(3-2) peak emission while the cyan star indicates the AGN position obtained from past literature. The beam size are represented by a grey ellipse. The CTAGN region is shown by a yellow contour. Note that not all sources exhibit a CTAGN yellow contour, as the integrated intensity values in these cases do not meet the threshold typically associated with CTAGN classification.

values for the sources are listed in Table 5. We compared the derived molecular hydrogen column densities, N_{H_2} with the X-ray-derived column densities, N_{H} from the 70-Month *Swift*/BAT catalogue, except for NGC 613, NGC 1097, and NGC 1808. For these sources, we used N_{H} values from previous literature: NGC 613 from She et al. (2017) as observed by *Chandra*, NGC 1097 from Asmus et al. (2015), and NGC 1808 from Heike & Awaki (2007).

In Figure 1, the CO moment 0 maps illustrate variations in

the morphology and concentration of dense CO gas near the nuclear region. From the I_{CO} we can infer the N_{H_2} values and identify the CTAGN regions. The yellow contours outline the boundaries of the CTAGN regions, visible in NGC 1068, NGC 4945, and NGC 6240. The high concentration of CO gas within these nuclear regions results in high N_{H_2} values that exceed the CTAGN threshold. This allows us to define the extent of the CTAGN region, characterised by substantial obscuration from dust and gas. In contrast, for other cases, the

Table 4. AGN Positions and Offsets

Source Name	AGN Position ¹		Peak Intensity ²		I_{CO} ($\times 10^3$ K kms ⁻¹)	Separation Offset (arcsec)	Ref. ³
	RA (h:m:s)	Dec (d:m:s)	RA (h:m:s)	Dec (d:m:s)			
Compton-Thick AGN							
Circinus Galaxy	14:13:09.948	-65:20:21.187	14:13:10.002	-65:20:20.670	2.0482	0.6173	1
NGC 1068	02:42:40.711	-00:00:47.940	02:42:40.710	-00:00:47.944	7.6091	0.0101	2
NGC 4945	13:05:27.477	-49:28:05.570	13:05:27.429	-49:28:05.947	8.5583	0.6039	3
NGC 5643	14:32:40.700	-44:10:27.800	14:32:40.704	-44:10:27.888	1.9713	0.1842	4
NGC 6240	16:52:58.896	+02:24:03.395	16:52:58.892	+02:24:03.832	9.2432	0.4278	5
NGC 7582	23:18:23.600	-42:22:13.000	23:18:23.645	-42:22:14.931	3.2204	0.8766	6
Non-Compton-Thick AGN							
NGC 613	01:34:18.19	-29:25:06.59	01:34:18.190	-29:25:06.690	3.6042	0.1000	7
NGC 1097	02:46:18.96	-30:16:28.900	02:46:18.973	-30:16:28.536	2.7749	0.3912	8
NGC 1566	04:20:00.397	-54:56:16.625	04:20:00.384	-54:56:16.560	0.8314	0.1269	9
NGC 1808	05:07:42.33	-37:30:45.88	05:07:42.327	-37:30:45.887	6.0154	0.0420	10
NGC 6300	17:16:59.473	-62:49:13.38	17:16:59.539	-62:49:13.980	2.0782	0.0649	11
NGC 7314	22:35:46.23	-26:03:00.90	22:35:46.193	-26:03:01.892	0.2371	0.2141	12

¹ Adopted AGN positions from past literature.

² Integrated CO(3-2) emission peak position.

³ Reference on the AGN position. (1) Greenhill *et al.* (2003a), (2) García-Burillo *et al.* (2019), (3) Greenhill *et al.* (1997), (4) Greenhill *et al.* (2003b), (5) Hagiwara *et al.* (2011), (6) Andonie *et al.* (2022), (7) Audibert *et al.* (2019), (8) Hummel *et al.* (1987), (9) Ricci *et al.* (2017), (10) Audibert *et al.* (2019), (11) García-Burillo *et al.* (2021), and (12) Evans *et al.* (2010)

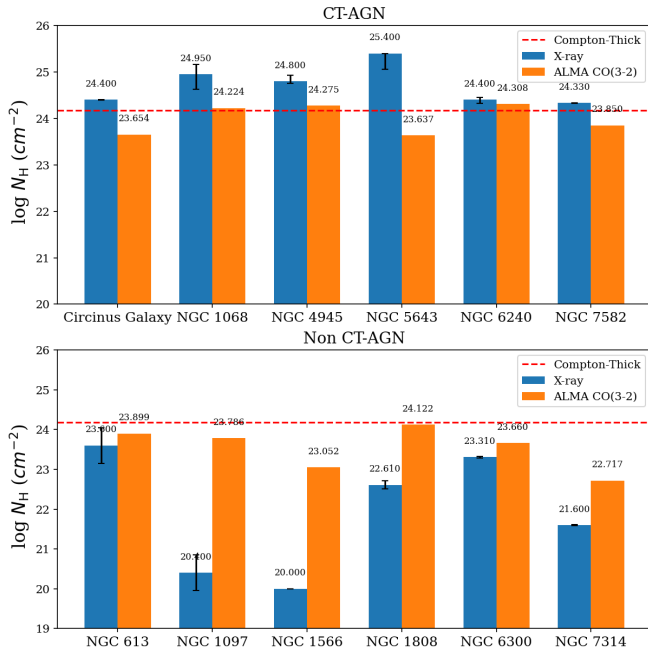


Figure 2. Column densities for molecular hydrogen, N_{H_2} derived using CO-to- H_2 conversion factor and total hydrogen, N_{Htotal} as inferred from X-ray. The red dotted line marks the CTAGN threshold.

absence of yellow contours indicates that the I_{CO} values do not surpass the CTAGN threshold, reflecting lower concentrations of molecular gas.

The results, shown in Figure 2, indicate that the molecular hydrogen column densities, N_{H_2} for CTAGNs are generally lower than the X-ray-derived column densities, N_{H} , consistent

Table 5. Molecular hydrogen column densities, N_{H_2} and logarithmic values for CTAGN and non-CTAGN. The N_{H_2} are given in units of 10^{23} cm⁻². The data highlights the relationship between sub-mm and X-ray observations, offering insights into the physical conditions within these galaxies.

Source Name	N_{H_2} ($\times 10^{23}$ cm ⁻²)	$\log_{10} N_{\text{H}_2}$ (cm ⁻²)	$\log_{10} N_{\text{H}}$ (cm ⁻²)
Circinus Galaxy	4.51	23.65	24.40 ¹
NGC 1068	16.74	24.22	24.95 ¹
NGC 4945	18.83	24.27	24.80 ¹
NGC 5643	4.34	23.64	25.40 ¹
NGC 6240	20.34	24.31	24.40 ¹
NGC 7582	7.09	23.85	24.33 ¹
NGC 613	7.93	23.90	23.60 ³
NGC 1097	6.10	23.79	20.40 ⁵
NGC 1566	1.13	23.05	20.00 ²
NGC 1808	13.23	24.12	22.61 ⁴
NGC 6300	4.57	23.66	23.31 ²
NGC 7314	0.52	22.72	21.60 ²

¹ Taken from Ricci *et al.* (2015)

² Taken from Ricci *et al.* (2017)

³ Taken from She *et al.* (2017)

⁴ Taken from Heike & Awaki (2007)

⁵ Taken from Asmus *et al.* (2015)

with previous studies. This discrepancy suggests that N_{H} may overestimate the total amount of obscuring material. The difference arises because X-ray and sub-mm observations trace different components and absorbers. X-ray emission is typically associated with inverse-Compton scattering originating in the corona, while sub-mm emission such as CO may arise from colder, absorbing gas. The lower N_{H_2} values in CT-AGN

could also result from the thick optical depth of the surrounding material, as CO emission, commonly used to infer H_2 densities, becomes optically thick, leading to underestimations of the N_{H_2} compared to X-ray-derived values, N_H that account for all type of hydrogen (atomic, HI and molecular, H_2) along the line of sight.

In contrast, non-CTAGN exhibit higher molecular hydrogen column densities, N_{H_2} , compared to the total hydrogen column densities, N_H . This can be attributed to their less dense surrounding environments, allowing for more effective tracing of H_2 through CO emission. Additionally, isotopologues of CO, such as ^{13}CO , are generally optically thin in less dense molecular clouds (Tan et al., 2011; Shimajiri et al., 2014; Barnes et al., 2020). In the case of CTAGN, the surrounding environment consists of highly dense regions, leading to high column densities. Under such conditions, CO emission can become saturated, limiting its effectiveness in tracing molecular gas. This phenomenon is demonstrated by Shetty et al. (2011), where they conducted radiative transfer modelling using magnetohydrodynamics (MHD) simulations of molecular clouds (MCs). Their study suggested that beyond a certain column density threshold, the CO line emission no longer correlates with the molecular mass. This limitation also extends to the estimation of H_2 column densities, as it relies on the same X_{CO} conversion factor. This supports the idea that the CO line may be optically thin in non-CTAGN regions.

The other possible factor for the discrepancy between N_{H_2} and N_H could be due to the total hydrogen column density, N_H derived from X-ray observations includes contributions from both atomic hydrogen (HI) and molecular hydrogen (H_2). In environments with significant amounts of HI, which is not traced by CO, the total hydrogen column density, $N_{H\text{Total}}$, can exceed the molecular hydrogen column density, N_{H_2} , derived from CO observations. This can be explained by the positive correlation between N_{HI} and N_H observed by Ostorero et al. (2010, 2017), where higher hydrogen column densities, N_H , measured from X-rays correspond to more significant HI detection. In this context, we can conclude that high N_H in CTAGN corresponds to higher HI detection, while lower N_H in non-CTAGN results in reduced HI detection. Thus, it will explain the discrepancy observed in this work.

In Fig. 2, most of the N_{H_2} does not exceed the threshold typically used to identify Compton-thick AGN (CTAGN), which is primarily defined through X-ray observations ($N_H \geq 1.5 \times 10^{24} \text{ cm}^{-2}$). This threshold represents the presence of highly dense regions in the nucleus, where the obscuring material around the AGN reaches extreme column densities. If N_{H_2} were to be used alone for identifying CTAGN, it may require a revised threshold. Only NGC 1068, NGC 4945, and NGC 6240 show N_{H_2} values that exceed this limit, indicating such dense regions in their nuclei. For both CTAGN and non-CTAGN, the difference between N_{H_2} and the threshold is relatively small, with values staying above $N_H = 10^{22} \text{ cm}^{-2}$. On the other hand, the total hydrogen column density, N_H shows a larger difference from the CTAGN threshold, especially for non-CTAGN sources.

In comparison with previous studies, the initial results of the

GATOS project (García-Burillo et al., 2021) also explored the variability of molecular gas masses within the nuclear region. They derived molecular hydrogen column densities, N_{H_2} , for several galaxies, some of which overlap with this study (e.g., NGC 1068, NGC 5643, NGC 6300, NGC 7314, and NGC 7582). The N_{H_2} values reported in their work are slightly lower than those presented here. This discrepancy could be attributed to the different CO-to- H_2 conversion factors, X_{CO} used in the analyses. While the GATOS project adopted a Milky Way conversion factor of $X_{CO} = 2 \times 10^{20} \text{ cm}^{-2} (\text{K km s}^{-1})^{-1}$, this study uses a slightly higher X_{CO} , resulting in marginally higher N_{H_2} values.

3.3 Correlation between N_{H_2} and N_H

In a previous study from Ostorero et al. (2017), they carried out a correlation analysis between radio column densities (N_{HI}) and X-ray column densities (N_H), suggesting a significant positive correlation, which implies as increasing value of X-ray observation, there will be increasingly detection in HI observation. In this work, to investigate the relationship between derived molecular hydrogen column density, N_{H_2} and total hydrogen column density, N_H , we performed a correlation analysis using three different correlation test, which is Kendall's correlation analysis, Spearman's correlation test, and Pearson's correlation analysis. Figure 3 displays the column densities plot between N_H and N_{H_2} on a log scale. with the linear regression fit line.

First, we investigate the correlation by applying Kendall's correlation test to the galaxy sample. The test shows that there is a weak positive monotonic association between N_H and N_{H_2} with Kendall's tau value, $\tau = 0.26$. This indicates that there is a slight tendency of higher N_H value to be associated with high N_{H_2} value. However, the correlation is not strong. Given the $P = 0.24$ is above 0.05, which common significance level, the relationship is not statistically significant. Thus, we are unable to claim there is a meaningful monotonic relationship between N_H and N_{H_2} . Further investigation with a larger dataset might be necessary to measure the significant relationship between these two column density.

To further study the correlation, we applied Spearman's correlation to the data sets, showing a moderate positive monotonic association between both column densities. The correlation value, $r_s = 0.42$ with $P = 0.17$ suggest that even with a positive moderate correlation, it is not strong enough to be considered reliable based on this sample alone. Larger data sets might be needed to confirm any potential relationship between these column densities. The correlation results shown by both tests agree with each other. Both tests show a positive monotonic correlation whereas a stronger correlation is shown by Spearman's test. The difference however slightly stronger than Kendall's test, which is expected because Spearman's test is more sensitive to monotonic relationships. Both p-values are greater than the common significance level of 0.05, indicating that neither test found a statistically significant correlation. However, the p-value from Spearman's test is closer to the significance threshold than that from Kendall's test, suggesting a marginally stronger but still statistically non-significant trend.

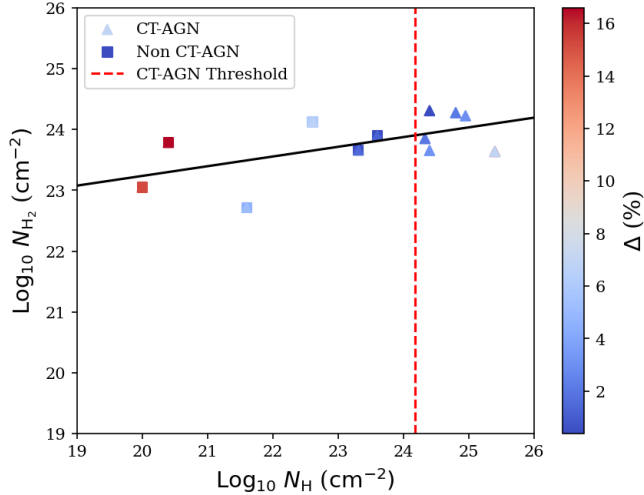


Figure 3. Correlation between the derived molecular hydrogen column density, N_{H_2} and total hydrogen column density, N_{Htotal} . The CTAGNs are marked with triangular shape and square for non-CTAGNs. The colour bar on the right shows the percentage difference of N_{H_2} from N_{Htotal} . The linear regression fit is represented by the solid black line.

This correlation has also been studied by García-Burillo *et al.* (2021), who reported a statistically significant positive relationship between these two variables, confirmed through Pearson’s correlation test. Other correlation tests such as Kendall and Spearman also suggest a similar result. The observed positive trend, though not statistically significant, suggests a possible association between dense gas (traced by CO(3-2)) and higher X-ray column densities. This could indicate the presence of molecular gas in regions with high obscuration, but further studies are required to confirm this relationship.

We investigate the relationship of these column densities by applying a regression analysis. We fit the data using linear regression fit, showing the linear relation given by;

$$\log_{10} N_{\text{H}_2} (\text{cm}^{-2}) = a \log_{10} N_{\text{H}} + b \quad (2)$$

as shown in figure 3. Although the correlation test shows a weak positive correlation, we performed the regression analysis to observe the dependency of N_{H_2} towards N_{H} . We obtained the slope, $a = 0.16$ with the intercept value, $b = 20.04$, showing alignment with the correlation, with the r-squared value expected to be low as weak or moderate correlation is shown. The R-squared value of 0.35 indicates a moderate fit, which could explain that the fit only captures some of the variability of the data while a significant amount of the remains unexplained. This preliminary analysis could potentially explore future works that can be done on the sample, to provide a better relationship of the column densities that are the main parameter of identifying CTAGN.

4. Conclusion

We present ALMA observations of CO(3-2) towards the central region of AGN samples, covering the Compton-thick and non-Compton-thick sources. We consider nearby AGN samples

based on their classification (CTAGN or non-CTAGN) and redshift, $z \leq 0.005$. We select the CTAGN samples from Ricci *et al.* (2017), in the 70-Month *SWIFT*/BAT catalogue, as well as the non-CTAGN sources. We also obtain samples from She *et al.* (2017) for both CTAGN and non-CTAGN. We search for ALMA CO(3-2) observations on the ALMA science archive and utilize the pipeline data provided, which results in having 6 CTAGNs and 6 non-CTAGNs. To obtain a good signal-to-noise ratio, we applied 3σ clipping before performing an integrated intensity map (moment 0). By using the Milky Way CO-to- H_2 conversion factor, we derive the molecular hydrogen column density (N_{H_2}), by taking the CO(3-2) peak integrated intensity. In order to study the correlation between molecular hydrogen column density (N_{H_2}) and total hydrogen column density (N_{H}) inferred from X-ray observation, we perform correlation test using Kendall’s and Spearman’s test. In addition, we fit a linear regression to explore the relationship between both column densities. Our main results are summarised as follows:

1. Dense Region Tracing: The dense regions traced by CO(3-2) exhibit emission peaks near the nucleus, which align with AGN locations identified in previous studies, with minimal offsets. This suggests the presence of concentrated dense regions around the nucleus, that could be associated with dusty molecular torus.
2. Comparison of N_{H_2} and N_{H} : In CTAGN samples, N_{H_2} tends to be lower than N_{H} . This discrepancy may arise from the different components producing the emissions, and possibly an underestimation of H_2 due to CO being optically thick in dense regions. Conversely, in non-CTAGN samples, N_{H_2} often exceeds N_{H} . This could be attributed to CO being optically thin in less dense regions, leading to higher estimates of N_{H_2} .
3. Correlation Analysis: Both Kendall’s (0.2595) and Spearman’s (0.4203) correlation tests indicate a positive monotonic relationship between N_{H_2} and N_{H} which agree with previous studies. This suggests that as N_{H} increases, N_{H_2} also tends to increase, with Kendall’s test showing a weaker association and Spearman’s test indicating a moderate positive correlation.
4. Statistical Significance: The p-values from both tests (Kendall’s: 0.2326, Spearman’s: 0.1737) indicate that the observed correlations are not statistically significant at the conventional threshold of 0.05. Therefore, the sample does not provide strong enough evidence to confirm a significant correlation between these column densities.

Future studies could focus on refining the CO-to- H_2 conversion factor by incorporating more precise measurements of the CO integrated intensity, I_{CO} and the molecular hydrogen column density, N_{H_2} . Additionally, exploring other methods for determining N_{H_2} , such as using other molecular lines or dust emission, could provide further insights into the obscuration properties of CTAGN.

Our findings contribute to a broader understanding of AGN environments and the complexities of measuring obscuration properties. Accurately determining column densities is crucial for distinguishing between different types of AGNs and under-

standing the nature of their central regions. Further exploration in this area, with more comprehensive datasets and refined methodologies, is essential for advancing our knowledge of the diverse and dynamic processes at play in these powerful cosmic phenomena.

Acknowledgement

This paper makes use of the following ALMA data: ADS/JAO.ALMA 2013.1.00813.S, 2015.1.00126.S., 2015.1.01286.S, 2015.1.00404.S, 2016.1.00232.S, 2016.1.00296.S, 2017.1.00082.S, and 2018.1.01236.S. ALMA is a partnership of ESO (representing its member states), NSF (USA) and NINS (Japan), together with NRC (Canada) and NSC, ASIAA (Taiwan) and KASI (Republic of Korea), in cooperation with the Republic of Chile. The Joint ALMA Observatory is operated by ESO, AUI/NRAO and NAOJ.

This research was supported by the Faculty of Science Research Grant (GPF081-2020) and the Universiti Malaya Special Grant (RUIP002-2023). We would like to extend our gratitude to both funding bodies for their generous support, which has been invaluable in advancing our research.

Data Availability

The data underlying this article are publicly available in the ALMA Science Archive at <https://almascience.nrao.edu/aq/>, and can be accessed with the following project IDs: 2013.1.00813.S, 2015.1.00126.S., 2015.1.01286.S, 2015.1.00404.S, 2016.1.00232.S, 2016.1.00296.S, 2017.1.00082.S, and 2018.1.01236.S.

References

- Agüero, E., Díaz, R., & Bajaja, E. 2004, *Astronomy & Astrophysics*, 414, 453 [6](#)
- Almeida, C. R., Bischetti, M., García-Burillo, S., et al. 2022, *Astronomy & Astrophysics*, 658, A155 [5](#)
- Alonso-Herrero, A., Pereira-Santaella, M., García-Burillo, S., et al. 2018, *The Astrophysical Journal*, 859, 144 [4, 7](#)
- Andonie, C., Bauer, F. E., Carraro, R., et al. 2022, *Astron. Astrophys.*, 664, A46 [10](#)
- Annuar, A., Gandhi, P., Alexander, D. M., et al. 2015, *The Astrophysical Journal*, 815, 36 [4](#)
- Antonucci, R. 1993, *Annu. Rev. Astron. Astrophys.*, 31, 473 [1](#)
- Asmus, D., Gandhi, P., Hönl, S. F., Smette, A., & Duschl, W. J. 2015, *Monthly Notices of the Royal Astronomical Society*, 454, 766–803 [9, 10](#)
- Audibert, A., Combes, F., García-Burillo, S., et al. 2019, *Astron. Astrophys.*, 632, A33 [5, 10](#)
- . 2021, *Astron. Astrophys.*, 656, A60 [6, 7](#)
- Awaki, H., Murakami, H., Leighly, K. M., et al. 2005, *The Astrophysical Journal*, 632, 793 [6](#)
- Barnes, A., Kauffmann, J., Bigiel, F., et al. 2020, *Monthly Notices of the Royal Astronomical Society*, 497, 1972 [11](#)
- Baumgartner, W., Tueller, J., Markwardt, C., et al. 2013, *The Astrophysical Journal Supplement Series*, 207, 19 [2](#)
- Bendo, G., Henkel, C., D’Cruze, M., et al. 2016, *Monthly Notices of the Royal Astronomical Society*, 463, 252 [3](#)
- Blackman, C. P. 1981, *Monthly Notices of the Royal Astronomical Society*, 195, 451–466 [5](#)
- Bland-Hawthorn, J., Gallimore, J., Tacconi, L., et al. 1997, *Astrophysics and Space Science*, 248, 9 [3](#)
- Bolatto, A. D., Leroy, A. K., Levy, R. C., et al. 2021, *Astrophys. J.*, 923, 83 [3](#)
- Braito, V., Reeves, J. N., Bianchi, S., Nardini, E., & Piconcelli, E. 2017, *Astron. Astrophys.*, 600, A135 [5](#)
- Carilli, C., & Walter, F. 2013, *Annual Review of Astronomy and Astrophysics*, 51, 105 [3](#)
- Chen, G., Bendo, G. J., Fuller, G. A., Henkel, C., & Kong, X. 2023, *Monthly Notices of the Royal Astronomical Society*, 525, 3645 [6](#)
- Circosta, C., Mainieri, V., Lamperti, I., et al. 2021, *Astron. Astrophys.*, 646, A96 [7](#)
- Comastri, A. 2004, *Compton-Thick AGN: The Dark Side of the X-Ray Background* (Springer Netherlands), 245–272 [2](#)
- Combes, F. 2023, *Galaxies*, 11, 120 [7](#)
- Combes, F., García-Burillo, S., Casasola, V., et al. 2014, *Astronomy & Astrophysics*, 565, A97 [6](#)
- da Silva, P., Menezes, R., Díaz, Y., et al. 2023, *Monthly Notices of the Royal Astronomical Society*, 519, 1293 [7](#)
- Davies, R., Mark, D., & Sternberg, A. 2012, *Astronomy & Astrophysics*, 537, A133 [2](#)
- Done, C., Madejski, G. M., & Smith, D. A. 1996, *Astrophys. J.*, 463, L63 [3](#)
- Emig, K. L., Bolatto, A. D., Leroy, A. K., et al. 2020, *The Astrophysical Journal*, 903, 50 [3](#)
- Emmanoulopoulos, D., McHardy, I., Vaughan, S., & Papadakis, I. 2016, *Monthly Notices of the Royal Astronomical Society*, 460, 2413 [7](#)
- Esposito, F., Vallini, L., Pozzi, F., et al. 2022, *Monthly Notices of the Royal Astronomical Society*, 512, 686 [2](#)
- . 2024, *Monthly Notices of the Royal Astronomical Society*, 527, 8727 [2](#)
- Evans, I. N., Primini, F. A., Glotfelty, K. J., et al. 2010, *Astrophys. J. Suppl. Ser.*, 189, 37 [10](#)
- Fabian, A. C. 1999, *Proceedings of the National Academy of Sciences*, 96, 4749–4751 [1](#)
- Freeman, K. C., Karlsson, B., Lynga, G., et al. 1977, *A&A*, 55, 445 [3](#)
- Galliano, E., & Alloin, D. 2008, *Astronomy & Astrophysics*, 487, 519 [6](#)
- García-Bermete, I., Alonso-Herrero, A., García-Burillo, S., et al. 2021, *Astronomy & Astrophysics*, 645, A21 [4](#)
- García-Burillo, S., Combes, F., Almeida, C. R., et al. 2016, *The Astrophysical Journal Letters*, 823, L12 [3, 6](#)
- García-Burillo, S., Viti, S., Combes, F., et al. 2017, *Astronomy & Astrophysics*, 608, A56 [3](#)
- García-Burillo, S., Combes, F., Ramos Almeida, C., et al. 2019, *Astron. Astrophys.*, 632, A61 [3, 10](#)
- García-Burillo, S., Alonso-Herrero, A., Ramos Almeida, C., et al. 2021, *Astron. Astrophys.*, 652, A98 [5, 7, 8, 10, 11, 12](#)
- García-Burillo, S., Hicks, E. K. S., Alonso-Herrero, A., et al. 2024, *Astronomy & Astrophysics*, 689, A347 [7, 8](#)
- Gatica, C., Demarco, R., Dole, H., et al. 2023, *Monthly Notices of the Royal Astronomical Society*, 527, 3006–3017 [1](#)
- Greenhill, L. J., Gwinn, C. R., Antonucci, R., & Barvainis, R. 1996, *Astrophys. J.*, 472, L21 [3](#)
- Greenhill, L. J., Kondratko, P. T., Lovell, J. E. J., et al. 2003a, *Astrophys. J.*, 582, L11 [10](#)
- Greenhill, L. J., Moran, J. M., & Herrnstein, J. R. 1997, *The Astrophysical Journal*, 481, L23–L26 [10](#)
- Greenhill, L. J., Booth, R. S., Ellingsen, S. P., et al. 2003b, *Astrophys. J.*, 590, 162 [3, 10](#)
- Hagiwara, Y., Baan, W. A., & Klöckner, H.-R. 2011, *Astron. J.*, 142, 17 [10](#)
- Hagiwara, Y., Horiuchi, S., Imanishi, M., & Edwards, P. G. 2021, *Astrophys. J.*, 923, 251 [3](#)
- Heckman, T. 1980, *Astronomy and Astrophysics*, vol. 87, no. 1-2, July 1980, p. 152-164. Research supported by the University of Washington., 87, 152 [5](#)
- Heckman, T. M., & Best, P. N. 2014, *Annual Review of Astronomy and Astrophysics*, 52, 589 [1](#)
- Heike, K., & Awaki, H. 2007, *Publications of the Astronomical Society of Japan*, 59, 531–540 [9, 10](#)

- Henkel, C., Mühle, S., Bendo, G., et al. 2018, *Astron. Astrophys.*, 615, A155 4
- Hicks, E. K. S., Davies, R. I., Malkan, M. A., et al. 2009, *Astrophys. J.*, 696, 448 2
- Ho, L. C. 2008, *Annu. Rev. Astron. Astrophys.*, 46, 475 5
- Hummel, E., van der Hulst, J. M., & Keel, W. C. 1987, *A&A*, 172, 32 10
- Imanishi, M., Nakanishi, K., Izumi, T., & Wada, K. 2018, *The Astrophysical Journal Letters*, 853, L25 3
- Izumi, T., Wada, K., Fukushige, R., Hamamura, S., & Kohno, K. 2018, *The Astrophysical Journal*, 867, 48 7
- Izumi, T., Kohno, K., Fathi, K., et al. 2017, *The Astrophysical Journal Letters*, 845, L5 5
- Jackson, F. E., Roberts, T. P., Gelbord, J. M., et al. 2010, in *AIP Conference Proceedings (AIP)* 2
- Jaffe, W., Meisenheimer, K., Röttgering, H., et al. 2004, *Nature*, 429, 47 3
- Jana, A., Chatterjee, A., Kumari, N., et al. 2020, *Monthly Notices of the Royal Astronomical Society*, 499, 5396 6
- Jones, G., Maiolino, R., Circosta, C., et al. 2023, *Monthly Notices of the Royal Astronomical Society*, 518, 691 7
- Kawamuro, T., Izumi, T., & Imanishi, M. 2019, *Publ. Astron. Soc. Jpn. Nihon Tenmon Gakkai*, 71 7
- Kollatschny, W., Weilbacher, P. M., Ochmann, M. W., et al. 2020, *Astron. Astrophys.*, 633, A79 4
- Komossa, S., Burwitz, V., Hasinger, G., et al. 2003, *Astrophys. J.*, 582, L15 4
- Koribalski, B. S., Staveley-Smith, L., Kilborn, V. A., et al. 2004, *The Astronomical Journal*, 128, 16 6
- Kormendy, J., & Ho, L. C. 2013, *ARA&A*, 51, 511 1
- Kormendy, J., & Ho, L. C. 2013, *Annual Review of Astronomy and Astrophysics*, 51, 511 1
- Kormendy, J., & Richstone, D. 1995, *ARA&A*, 33, 581 1
- Lamperti, I., Saintonge, A., Koss, M., et al. 2020, *Astrophys. J.*, 889, 103 7
- Liszt, H. 2021, *The Astrophysical Journal*, 908, 127 2
- Marinucci, A., Bianchi, S., Matt, G., et al. 2015, *Monthly Notices of the Royal Astronomical Society: Letters*, 456, L94–L98 3
- Merloni, A., & Fabian, A. 2001, *Monthly Notices of the Royal Astronomical Society*, 328, 958 1
- Mezcua, M., Prieto, M. A., Fernández-Ontiveros, J. A., & Tristram, K. R. W. 2016, *Monthly Notices of the Royal Astronomical Society: Letters*, 457, L94–L98 3
- Miyamoto, Y., Nakai, N., Seta, M., et al. 2017, *Publications of the Astronomical Society of Japan*, 69, doi:10.1093/pasj/psx076 5, 7
- Morris, S. L., & Ward, M. J. 1985, *Monthly Notices of the Royal Astronomical Society*, 215, 57P 6
- Nagao, T., Taniguchi, Y., & Murayama, T. 2000, *The Astronomical Journal*, 119, 2605 6
- Nemmen, R. S., Storchi-Bergmann, T., Yuan, F., et al. 2006, *The Astrophysical Journal*, 643, 652 5
- Ostorero, L., Morganti, R., Diaferio, A., et al. 2017, *Astrophys. J.*, 849, 34 11
- Ostorero, L., Moderski, R., Stawarz, L., et al. 2010, *Astrophys. J.*, 715, 1071 11
- Pfuhl, O., Davies, R., Dexter, J., et al. 2020, *Astronomy & Astrophysics*, 634, A1 3
- Phillips, A. C. 1993, *Astronomical Journal (ISSN 0004-6256)*, vol. 105, no. 2, p. 486-498., 105, 486 6
- Phillips, M., Charles, P., & Baldwin, J. 1983, *Astrophysical Journal, Part 1*, vol. 266, Mar. 15, 1983, p. 485-501., 266, 485 6
- Prieto, M. A., Fernández-Ontiveros, J. A., Bruzual, G., et al. 2019, *Monthly Notices of the Royal Astronomical Society*, 485, 3264–3276 5
- Prieto, M. A., Meisenheimer, K., Marco, O., et al. 2004, *Astrophys. J.*, 614, 135 3
- Rahmani, S., Lianou, S., & Barmby, P. 2016, *Monthly Notices of the Royal Astronomical Society*, 456, 4128–4144 8
- Regan, M. W., & Mulchaey, J. S. 1999, *The Astronomical Journal*, 117, 2676 5
- Ricci, C., Ueda, Y., Koss, M. J., et al. 2015, *The Astrophysical Journal*, 815, L13 2, 10
- Ricci, C., Trakhtenbrot, B., Koss, M. J., et al. 2017, *The Astrophysical Journal Supplement Series*, 233, 17 2, 10, 12
- Rivers, E., Baloković, M., Arévalo, P., et al. 2015, *Astrophys. J.*, 815, 55 5
- Salak, D., Nakai, N., Hatakeyama, T., & Miyamoto, Y. 2016, *The Astrophysical Journal*, 823, 68 6
- Schulz, H., Knake, A., & Schmidt-Kaler, T. 1994, *Astronomy and Astrophysics*, Vol. 288, p. 425-432 (1994), 288, 425 6
- Schurch, N., Roberts, T., & Warwick, R. 2002, *Monthly Notices of the Royal Astronomical Society*, 335, 241 3
- Sérsic, J., & Pastoriza, M. 1965, *Publications of the Astronomical Society of the Pacific*, 77, 287 6
- She, R., Ho, L. C., & Feng, H. 2017, *The Astrophysical Journal*, 835, 223 3
- She, R., Ho, L. C., & Feng, H. 2017, *ApJ*, 835, 223 9, 10, 12
- Shetty, R., Glover, S. C., Dullemond, C. P., et al. 2011, *Mon. Not. R. Astron. Soc.*, 415, 3253 11
- Shimajiri, Y., Kitamura, Y., Saito, M., et al. 2014, *Astronomy & Astrophysics*, 564, A68 11
- Shobbrook, R. 1966, *Monthly Notices of the Royal Astronomical Society*, 131, 365 6
- Silver, R., Torres-Albà, N., Zhao, X., et al. 2023, *Astronomy & Astrophysics*, 675, A65 2
- Silverman, J. D., Mainieri, V., Ding, X., et al. 2023, *The Astrophysical Journal Letters*, 951, L41 2
- Smajić, S., Moser, L., Eckart, A., et al. 2015, *Astronomy & Astrophysics*, 583, A104 6
- Solomon, P. M., Barrett, J., Sanders, D. B., & de Zafra, R. 1983, *ApJ*, 266, L103 8
- Stauffer, J. R. 1982, *Astrophysical Journal, Part 1*, vol. 262, Nov. 1, 1982, p. 66-80., 262, 66 6
- Storchi-Bergmann, T., Baldwin, J. A., & Wilson, A. S. 1993, *Astrophysical Journal, Part 2-Letters (ISSN 0004-637X)*, vol. 410, no. 1, p. L11-L14., 410, L11 5
- Tan, Q.-H., Gao, Y., Zhang, Z.-Y., & Xia, X.-Y. 2011, *Research in Astronomy and Astrophysics*, 11, 787 11
- Torres-Albà, N., Marchesi, S., Zhao, X., et al. 2023, *Astronomy & Astrophysics*, 678, A154 2
- Treister, E., Messias, H., Privon, G. C., et al. 2020, *The Astrophysical Journal*, 890, 149 4
- Trippe, M., Crenshaw, D., Deo, R., et al. 2010, *The Astrophysical Journal*, 725, 1749 6
- Tristram, K. R., Impellizzeri, C. V., Zhang, Z.-Y., et al. 2022, *Astronomy & Astrophysics*, 664, A142 7
- Tsai, M., Hwang, C.-Y., Matsushita, S., Baker, A. J., & Espada, D. 2012, *The Astrophysical Journal*, 746, 129 7
- Tully, R. B., Courtois, H. M., & Sorce, J. G. 2016, *The Astronomical Journal*, 152, 50 6
- Turner, T., George, I., Nandra, K., & Mushotzky, R. 1997, *The Astrophysical Journal Supplement Series*, 113, 23 7
- Wang, J., Fabbiano, G., Karovska, M., Elvis, M., & Risaliti, G. 2012, *The Astrophysical Journal*, 756, 180 3
- Wilson, A. S., Shopbell, P. L., Simpson, C., et al. 2000, *Astron. J.*, 120, 1325 3
- Wilson, C. D., Warren, B. E., Israel, F. P., et al. 2009, *Astrophys. J.*, 693, 1736 3
- Wold, M., Lacy, M., Käuff, H. U., & Siebenmorgen, R. 2006, *Astron. Astrophys.*, 460, 449 5
- Yaqoob, T., Serlemitsos, P., Turner, T., George, I., & Nandra, K. 1996, *The Astrophysical Journal*, 470, L27 7